This is a preprint, the final version is subject to change, of the American Mineralogist (MSA)
Cite as Authors (Year) Title. American Mineralogist, in press.
(DOI will not work until issue is live.) DOI: http://dx.doi.org/10.2138/am-2015-5056

MS 5283 R3: Name on machine: Lin Part R3

Linear partitioning in binary solutions: a review with a novel partitioning array

S. A. Morse*

Department of Geosciences, University of Massachusetts, 611 North Pleasant Street, Amherst, Massachusetts, 01003-9297, U. S. A.

*E-Mail: tm@geo.umass.edu

Revision 3
8 January 2015

ABSTRACT

Linear partitioning refers to a graphical plot of a partition ratio $D \leq 1.0$ against a composition ratio X_2 given as the mole fraction of a refractory component 2. When this plot is linear from D =1.0, X_2 = 0.0, its intercept at X_2 = 1.0 is a value on the D scale here identified as the value of the exchange coefficient K_D. The plot is generated from phase compositions 1,2 in states L_V or L_S or S_S depending on whether the system is a boiling mixture, a melting equilibrium, or a solid-solid equilibrium. The linear partitioning equation so generated is a mathematical description of a binary solution loop, and it has the form y = ax + b where y ≡ D, a ≡ K_D, x ≡ X_2 , and b = 1-x ≡ 1-X_2. In practice, the linearity is tested by regressing values of D against X_2 to find the intercept K_D. If linearity occurs, the system is a binary solution loop; if it does not occur, the system is not a binary loop. Strict linearity is not always observed even in true binary solutions; in such cases the path to K_D may be either segmented or moderately curved. Such is the case with the melting equilibria of both plagioclase and olivine, possibly a clue to the non-ideality of solution. Loop width is an inverse function of K_D, and can vary with pressure as in the case of plagioclase in troctolites and gabbros. Systems with two loops joined at a common minimum or maximum are called

Always consult and cite the final, published document. See http://www.minsocam.org or GeoscienceWorld

azeotropes and all of them show linear partitioning. Sanidine crystalline solutions form a classic example of such behavior. When the system An-Ab is revisited to repeat the Bowen thermodynamic calculation from the latent heats of fusion with modern data, the array shows a single modest curvature. The monoclinic pyroxene pairs augite and pigeonite form a binary loop; augite - orthopyroxene does not. The olivine compositions of rocks in the Kiglapait intrusion follow a linear partitioning line with $K_D = 0.26$ for data above fifty percent crystallized (50 PCS). All the rocks below 50 PCS occupy a new trend in the linear partitioning diagram. This trend is anchored at $D = 0.0$, $X_2^S = 1.0$ and runs to the calculated liquid composition at its intercept with the $D = 1.0$ upper bound.. The new trend is the graphical solution to the ambient liquid composition given the crystal composition and the value of K_D. Its origin involves at least three working hypotheses not yet fully explored.

Key words: Binary solutions, linear partitioning, phase equilibrium, plagioclase, olivine, augite, melting, crystallization.

INTRODUCTION

Linear partitioning in binary solutions is a device by which fractionation or reactive equilibrium processes can be explored mathematically and compared with natural or experimental results. Linearity occurs when a ratio of mole fractions is a linear function of composition in a binary solution. If this condition fails to occur, the object studied is not a binary solution. In this review the intent is to organize previous derivations and expositions into a concise collective whole with examples drawn from boiling mixtures, feldspars, pyroxenes and olivine. This exercise results in a geometrical solution to the problem of finding the liquid composition of a binary mixture when the crystal composition and crystal-liquid exchange coefficient are known or given.. It is then possible to introduce a new and unforeseen application that defines a liquid composition but has plausible origins still being explored.

Abbreviations used in this paper are listed in Table 1.

Always consult and cite the final, published document. See http://www.minsocam.org or GeoscienceWorld

GENERAL CONSIDERATIONS

The linear partitioning equation is the mathematical description of a binary solution loop. It is the simple equation $y = ax + b$ where y is the partition coefficient, a is the exchange coefficient, x (in melting equilibria) is the refractory crystal composition, and $b = 1\text{-}x$. This equation first appeared in a discussion of olivine in the Kiglapait Intrusion (Morse, 1996) in which its chief purpose was to aid in the calculation of Rayleigh fractionation by iteration in small steps. This operation was accomplished by adjusting the partition coefficient at every step of the iteration using the current value of the exchange coefficient. For melting equilibria the linear partitioning equation takes the form

$$D = K_D \cdot X_2^S + X_1^S \qquad \textbf{(1)}$$

where D is the partition coefficient set ≤ 1.0 and defined as X_1^S/X_1^L, X is a mole fraction, S is a solid crystalline solution, L is liquid, component 1 is the low-temperature melting component and component 2 the corresponding high-temperature melting component. The *exchange coefficient* K_D is the double ratio of moles n: $(n1/n2)^S$ so formed also as to be ≤ 1.0. The equation is generally used by regressing values of D against X_2^S to test for unity at $X_2^S = 0$ and to find the intercept K_D at $X_2^S = 1.0$.

This formulation, developed more fully below, was then subsequently tested against a variety of melting equilibria, boiling mixtures (L-V equilibria), and solid-solid assemblages stimulated by the suggestion of *garnet-chlorite* or *biotite-garnet* Mg-Fe exchange within multi-component systems (Ramberg, 1952). The history after the olivine application is contained in papers by Morse (1997, 2000, 2001) and summarized in Morse (2013).

Some results of these explorations are listed in Table 2. They run from the standards of igneous petrology in the melting loops of olivine, plagioclase, alkali feldspars and pyroxenes, to systems with water, systems at pressure, solid-solid mantle equilibria such as magnesiowüstite, spinel, augite-olivine equilibria, chlorite-garnet and high-temperature biotite-garnet. Another

Always consult and cite the final, published document. See http://www.minsocam.org or GeoscienceWorld

result in multi-component systems is the increase of K_D with pressure for plagioclase crystallizing with pyroxene and olivine, to a value exceeding 1.0 at 15 kbar (Morse, 2013), a result that would suggest the presence of an azeotrope (a melting maximum) except that it is in fact the breakdown of plagioclase to spinel, garnet, and two aluminous pyroxenes (McIntosh, 2009).

For *L-V* and *S-S* equilibria the notation of linear partitioning needs to be changed to be more general in terms of components and ratios. This is done in Morse (2000) and need not concern us in the present mineralogical context. There are attendant thermodynamic considerations, developed in that paper as well; these are of secondary interest here.

SYSTEMATICS OF LINEAR PARTITIONING

Notation

The conventions of Beattie et al. (1993) are followed herein. Problems eternally arise because in some conventions the *partition coefficient D* and the *exchange coefficient* K_D have been interchanged, at least in name. The distinction can be important, because in the convention adopted here the partition coefficient can have a thermal dimension whereas the exchange coefficient is rigorously athermal. The partition coefficient is akin to the Nernst *distribution coefficient* and has often been called that in the older geochemical literature.

ALGEBRAIC DERIVATION FOR MELTING OF CRYSTALLINE SOLUTIONS

Here we derive equation (1) for melting equilibria so as to clarify each step of the development. For a solid phase *S* and liquid phase *L* we define the *partition coefficient D* set always to be ≤ 1.0 and hence

$$D_{X_1}^{S/L} = X_1^S / X_1^L \quad \textbf{(2)}$$

Always consult and cite the final, published document. See http://www.minsocam.org or GeoscienceWorld

where the *mole fraction* X_1 is the normalized fraction of the low-melting component (1), i.e.

$$X_1 = n_1 / (n_1 + n_2) \quad \textbf{(3)}$$

where n is the number of moles and component (2) is the high-melting component. The notation may apply in other cases with different names, to units of mass, gram-atoms, or oxygen-normalized cations. Defining the *exchange coefficient* K_D as

$$K^{S/L}_{D(n1/n2)} = \frac{(n_1 / n_2)^S}{(n_1 / n_2)^L} \quad \textbf{(4)}$$

and using this, we obtain

$$D^{S/L}_{X_1} = K^{S/L}_{D_{1/2}} \cdot (1 - X_1^S) + X_1^S \quad \textbf{(5)}$$

$$= (K_D \cdot X_2^S) + X_1^S \quad \textbf{(6)}$$

which is the linear partitioning equation relating the partition coefficient to the exchange coefficient via the crystal compositions (Morse, 1996).

Proof

The above result is shown to be true as follows, using for petrologic interest a familiar case of olivine melting (Morse, 1997). Defining

$$K_D \equiv \frac{(n_{Fe} / n_{Mg})^S}{(n_{Fe} / n_{Mg})^L} = \frac{(X^S_{Fe} / X^S_{Mg})}{(X^L_{Fe} / X^L_{Mg})} = \frac{X^S_{Fa} / (1 - X^S_{Fa})}{X^L_{Fa} / (1 - X^L_{Fa})} \quad \textbf{(7)}$$

Always consult and cite the final, published document. See http://www.minsocam.org or GeoscienceWorld

we have

$$K_D(X_{Fa}^L)\cdot(1-X_{Fa}^S)=X_{Fa}^S(1-X_{Fa}^L) \quad \textbf{(8)}$$

$$K_D(X_{Fa}^L)-K_DX_{Fa}^L\cdot(X_{Fa}^S)=X_{Fa}^S-X_{Fa}^SX_{Fa}^L \quad \textbf{(9)}$$

$$K_D-K_DX_{Fa}^S=\frac{X_{Fa}^S}{X_{Fa}^L}-X_{Fa}^S \quad \textbf{(10)}$$

and finally

$$K_D(1-X_{Fa}^S)=D-X_{Fa}^S \quad QED \quad \textbf{(11)}$$

Discussion and an application

The geometric expression of this result is illustrated in Fig. 1. If the system is a true binary loop then the partitioning is strictly linear from (0,1) to the value of K_D at $X_2^S = 1.0$. This was found to be almost true for olivine as computed by Bradley (1962) from the data of Bowen and Schairer (1935), but the actual data points for Fe-rich olivines defined a slightly variable array above the linear approximation (Morse, 1997 Fig. 1). The result is that in the real case the implied value of K_D changes from 0.227 at pure Fo to 0.266 at pure Fa. Although this would seem to be a trivial difference, it is probably not erroneous. A more significant effect on olivine partitioning is the structure of the liquid, to be discussed.

Loop width and K_D

The exchange coefficient K_D carries the essential feature of the binary loop because its value relates inversely to the width of the loop. Thus a low value of K_D describes a wide or fat loop with a large distance between the solidus and liquidus, whereas a high value of K_D describes a

Always consult and cite the final, published document. See http://www.minsocam.org or GeoscienceWorld

127 narrow loop. It helps to remember this relationship if note is taken that a K_D of 1.0 means a loop
128 with no width at all: a single line. This limit is actually achieved in azeotropes, systems with a
129 maximum or minimum, as we shall see. And of course, the lower limit of $K_D = 0$ describes a
130 rectangular box, hence no longer a loop. This loop-width feature of K_D is quantified for an
131 arbitrary special case in Fig. 2a. Figure 2b describes another feature of K_D, the pressure effect
132 on natural plagioclase feldspar.

133 ## APPLICATION TO BOILING MIXTURES

134 In an earlier treatment (Morse, 2000) the formulation of equation (5) was expanded for
135 boiling mixtures to erect a general notation for components (*i, j*) in place of (1,2) and states of
136 matter (*L,V*) for boiling mixtures. An example of a rigorously linear result is shown in Fig. 3
137 here. The cited paper also illustrated this notation in a reverse linear partitioning diagram, and
138 one example of a boiling mixture was shown in three frames: one with *Xj* in the liquid; one with
139 *Xj* in the vapor, and a third with a comparison of both Dj^{-1} and *Dj*, plotted against the vapor
140 composition. In that case the inverse formulation Dj^{-1} is linear and the direct formulation *Dj* is a
141 concave-up curve. This reference also showed a pronounced failure of linear partitioning in a
142 boiling mixture (CCL4 - Acetone at 0.600 bar), reproduced here as Fig. 4. In this case the strong
143 curvature of the data require a distorted loop with a nearly isothermal tail. The reference also
144 lists the outcome of examining 11 boiling mixtures among which five clearly failed to yield
145 linear partitioning.

146 ### Azeotropes

147 An azeotrope is a pair of interconnected binary solutions melting (condensing) at a common
148 point that is either a thermal (pressure) minimum or a maximum. Familiar examples in petrology
149 are the alkali feldspars. The application of linear partitioning to azeotropes requires dual
150 partitioning equations; the identities of components *i* and *j* are switched at the azeotropic point
151 (AP). Each regression is carried out independently and each finds a unique value of the
152 composition of the AP. These are averaged if required to find a joint solution, and the treatment

Always consult and cite the final, published document. See http://www.minsocam.org or GeoscienceWorld

of regressions to find the intercepts at each end member is discussed in the referenced article.

Continuing the literature search in boiling mixtures, of six azeotropic mixtures examined, all were linear, including both *T*-*X* and *P*-*X* variations. Typical correlations found for azeotropes have a correlation coefficient $R^2 > 0.99$. Because of the common azeotropic point, all azeotropes are made of binary solution loops. This result leads us back to familiar silicate systems.

ALKALI FELDSPARS: THE AZEOTROPIC SYSTEM Ab-Or

Azeotropic systems are typically non-ideal mixtures. A major contribution to the science of mixing properties in crystalline solutions was made by Waldbaum (1969) on the system NaCl - KCl and by Waldbaum and Thompson (1969) on sanidine crystalline solutions in the system $NaAlSi_3O_8$-$KAlSi_3O_8$, Albite-Orthoclase, Ab-Or. Because their solution models are so elegant, they make especially good examples of linear partitioning. Both systems were figured and described in Morse (2000); a new version of the Ab-Or system is shown here in Fig. 5, using all data from the original Table 2 of Waldbaum and Thompson (1969). Part A of the figure shows the *T*-*X* binary loop with a minimum, the azeotropic point AP at 1063 °C. The temperatures are uncorrected to Ab = *L* at 1100 °C (see the An-Ab system discussed below). The sanidine (Or component) limb is metastable with respect to leucite plus liquid, caused by the incongruent melting of Or (*e.g.*, Morse, 1994). Part B of Fig. 5 is the linear partitioning diagram showing the separate treatments of the two limbs of the binary loop. Here the protocols described above are put to work: the identities of X_1 and X_2 (reverting to the previous notation) are switched at the AP and separate regressions are run on each. This interchange means that, for example in the Ab-rich limb, X_2 = Ab and X_1 = Or; as always component (1) is the low-*T* component. For each limb the linear partitioning equation is modified so that $D = K_D X_2^S + (a \cdot X_1^S)$ where *a* is a fitting parameter, with calculated values shown in the figure. The values of K_D are received in the regressions. As commonly found, the values at the extrema of composition are highly sensitive to rounding error and exact coincidence with the regressed limit is rare. In this example the last

Always consult and cite the final, published document. See http://www.minsocam.org or GeoscienceWorld

data points are omitted from the regression, which has in both cases $R^2 = 0.999$.

EFFECT OF A THIRD COMPONENT

Simple binary solutions are ideal systems for rigorous understanding of the geometric and physical principles underlying their behavior. In many cases, the addition of a third component would not have a profound effect on the binary equilibria. For example, the addition of quartz to the system Ab-Or cited above does not by itself change the fundamentally azeotropic nature of the binary loop, because silica is common to both binary components in similar ways. On the other hand, the addition of a new component contained in only one of the binary pairs is likely to have a significant effect. Such is the effect of adding a Ca-pyroxene to plagioclase. This classic example of the system Di-An-Ab due to Bowen (1915) furnishes yet another linear partition of interest for the information it yields. The ternary diagram in Fig. 6a (inset) reminds us of the single cotectic running through the ternary with diopside crystallizing on one side and plagioclase on the other side.

Readers may recall that the liquid in the plagioclase field runs sharply toward the cotectic, but when that is reached, the liquid makes a hard turn towards Ab and runs directly away from both of the Ca-rich phases on the Di-An sideline. Accordingly, the fractionation toward Ab speeds up greatly when the liquid is multiply-saturated. But we diverge from the task at hand. The main feature of Fig. 6a is the *T-X* plot showing the steepening toward the Ab end and in particular the incomplete termination near Ab. This occurs because when the liquid reaches the sideline Ab-Di it leaves the ternary plane into multicomponent space involving all components of all three phases liquid, pyroxene, and plagioclase. The details need not concern us here, but of some interest is the composition of the plagioclase when the liquid reaches the sideline.

Bowen's tools and his fine-grained crystals were not well suited to this determination. Figure 6b contains the answer. Bowen's original three-phase triangle determinations yield the points marked with filled black rectangles. These eight points were found through a series of subtle and

Always consult and cite the final, published document. See http://www.minsocam.org or GeoscienceWorld

canny experiments involving several bulk compositions and the beginning of melting. In two experiments using electron microprobe determinations by Kushiro (1973), shown as filled triangles, one lies exactly on Bowen's line and another well off the line despite a long run time. The line is the linear regression on all but two points, yielding a value of $K_D = 0.26$. The upper end of the correlation misses the upper corner and instead lands at $D = 0.975$. From the partitioning equation the limiting plagioclase composition is An 9, and that is where the *T-X* diagram places it. The loop is not strictly binary, but its treatment with linear partitioning brings out a useful quantification of its imperfection. Of major interest is the value of $K_D = 0.26$ given by the regression, because this gives us a best 1-atm value for plagioclase - liquid partitioning in a pyroxene - saturated system, corresponding to the nature of many mafic igneous rock types including norite and gabbro. This value serves as the anchor for the effect of pressure on the value of K_D in pyroxene-saturated plagioclase previously mentioned and as shown in figures 5 and 7 of Morse (2013).

In summary, the addition of a third component can change the partitioning of a binary loop and needs to be considered when seeking information about the behavior of liquids in natural systems.

IDEALITY IN BINARY SOLUTIONS

Ideal solutions evidently display linear partitioning. Non-ideal solutions might not be expected to do so. Nevertheless, as the Ab-Or system has dramatically shown, linear partitioning can occur even in an azeotrope for which the substantial mixing energies were famously calculated from thermodynamic principles.

A system at equilibrium has a locally minimized Gibbs free energy related to the exchange coefficient and the activity coefficient by

$$\ln K_D = -\frac{\Delta G^\circ}{RT} - \ln K_\gamma \quad \textbf{(12)}$$

Always consult and cite the final, published document. See http://www.minsocam.org or GeoscienceWorld

where γ is the activity coefficient and $K\gamma$ is the ratio of activities in one phase divided by the ratio of activities in the other phase when there is a simple equilibrium of the form a = b. For the case $K\gamma = 1.0$, the solution is said to be ideal, but alternatively their ratio is fortuitously equal to 1.0. In the case of the azeotropes (for which K_D is a constant for each individual side), a practical result must be the assumption that the activity coefficient is fortuitously equal to 1.0. In this case, the linearity of the partition coefficient against composition says nothing whatever about the individual activities of the conjoined binary solutions.

The plagioclase feldspar system is expected to be non-ideal from the behavior of Al^{3+} in An and Ab and the disorder of AlSi in anorthite (*e.g.*, Mysen and Richet, 2005). In an earlier treatment (Morse, 1997) it was shown that for Bowen's (1913) system An-Ab the partitioning was not linear, but curved, concave-up, with an intercept at $K_D = 0.282$. It was also shown that the departure from linearity became less at high pressure. We may now revisit this problem with a brief review of Bowen's analysis of the data, in which possibilities arise for retrieving fundamental information from linear partitioning.

MELTING IN THE SYSTEM AN-AB AT 1-ATM

Introduction

It is now a century plus two years since Bowen (1913) published "The melting phenomena of the plagioclase feldspars," a treatise that is surely the rock-bottom foundation of all modern igneous petrology. In this document, Bowen not only determined the liquidus and solidus curves and temperatures of the plagioclase loop, but also used thermodynamics to analyze the result. In this exercise, he proceeded not merely to assume the provisional enthalpies of fusion of An and Ab, but ultimately to *extract* one of these values from the experimental array. He then conducted an error analysis (Bowen's Table V) by changing each value of the enthalpy of fusion by 10% and recalculating the implied temperature for each of the liquidus and solidus. In this exercise he showed that the result of the 10% variation was "well beyond the limits of error of the temperature measurements."

Always consult and cite the final, published document. See http://www.minsocam.org or GeoscienceWorld

In passing, it is worth our notice to cite two of Bowen's classic statements, as follows:

"van Laar derives a more rigid relation which contains factors for the heats of mixing in both phases, but in its application he finds it necessary to neglect these and the equations then reduce substantially to the form given above" (page 590)[1]

And again from p. 590:

"If the calculated mean molal latent heat of melting of anorthite is divided by the formula weight, the result is 29000 ÷ 278 = 104.2. Åkerman and Vogt have found by direct measurement that the latent heat of melting of anorthite is 105 cal. per gram, which agrees well with the calculated value. The extraordinary agreement is, of course, in part pure accident."

NB: "in part"

Bowen's Figure 8 shows the calculated liquidus and solidus curves for plagioclase along with the experimental data. All the points lie on the lines except three solidus points close to the Ab endmember, which lie at lower temperatures than observed.

Present work

The current exercise to find a modern working diagram for plagioclase is basically that of Bowen (1913). The history of the albite melting point is interesting. With much struggle, Bowen concluded that this end member melted at 1100 ± 2 °C. This result was later changed to 1118 °C by Schairer and Bowen (1956), and then returned to 1100 °C by Anovitz and Blencoe (1999; see discussion by Lange, 2003). The melting point of An (1553 °C instead of Bowen's 1550 °C) is taken from Osborn (1942). The liquidus and solidus curves were first recalculated from the latent heats of fusion using Bowen's value for ΔH_f (An) = 121.3 kJ and the value for ΔH_f (Ab) = 59.28

[1] Bowen does not provide a reference for van Laar, but presumably refers to the noteworthy paper of 1908 now referenced here. Note that the problem of non-ideal mixing goes back to van Laar, along with the partial solution (i.e.: ignore it).

Always consult and cite the final, published document. See http://www.minsocam.org or GeoscienceWorld

kJ (compared to Bowen's 53.3 kJ) from Robie et al. (1978). The **liquidus** curve (Fig. 7a) so calculated fits Bowen's data almost exactly. The **solidus** curve is continuous (Fig. 7a) instead of the former straight line at high values of An followed by a curve to the Ab end point (*e.g.*, Morse, 1994 p. 63).

There is an objection to the use of modern data for the latent heats of fusion when they were determined on glass (quenched melt) which is frozen in at the glass transition. In consequence, the heat of fusion calculated from solution calorimetry of glasses, as done in the recent literature including Robie et al. (1978), is not the ΔH of melting (*e.g.*, Richet and Bottinga, 1986). There is, however, a purely empirical approach in which we may test the results of new data inputs against the experimental *T*-*X* data of Bowen (1913). This procedure reflects the original use of the phase diagram from which Bowen extracted at least one of the heats of fusion, as discussed above.

Still using Bowen's ΔH_f (An) = 121.3 kJ, the partitioning plot is linear in two segments joined at An_{60} (dotted line in Fig. 7b) and a K_D value of 0.3. However, using instead an updated value ΔH_f (An) = 134.6 kJ (Navrotsky et al. 1980), the partitioning line becomes a single curve with K_D = 0.276, as shown by the heavy solid line in Fig. 7b. As also shown in the figure, the data near the An end of the array are typically scattered because an error of only 0.001 in X_{An} has a large effect on the result. This marriage of old and new data continues the Bowen principle of testing for a thermodynamic quantity by fitting to the experimental data. In this comparison there is no empirical evidence for rejecting the 1980 result, despite its origin from glass. As a result, we have a reasonable interim model for plagioclase alone to compare with more complex bulk compositions.

SOLID-SOLID EQUILIBRIA: A PYROXENE SOLVUS

The system Wo-En-Fs furnishes in its lower half the familiar **pyroxene quadrilateral** bounded by the Mg-Fe solutions Diopside-Hedenbergite at the top (X_{Wo} = 0.5) and Enstatite-Ferrosilite at the bottom (X_{Wo} = 0). This diagram features a three - dimensional solvus whose limbs separate Ca-rich augites from Ca-poor pigeonites accompanied by even Ca-poorer

Always consult and cite the final, published document. See http://www.minsocam.org or GeoscienceWorld

orthopyroxenes. The solvus has the form of an eastward-plunging anticline that becomes narrower with pressure as the temperatures rise (Lindsley, 1983). Two partitioning plots taken graphically from Fig. 9a of Lindsley (1983) are shown in Fig. 8. In the upper panel the augite-pigeonite pairs show an ideal linear partitioning relationship with a value of $K_D = 0.74$ received from the regression, and an exact intercept at $D = 1.0$. This result is not unsurprising for the two structurally-similar monoclinic crystal species. Using the same original diagram we find that the augite-orthopyroxene partitioning (Fig. 8b) is erratic – that is, the data points are randomly distributed without slope and a rough estimate of $D = K_D = 0.94$. For these two mixed-crystallographic phases there is no binary solution loop and the relationships are not athermal. They are not well-related to temperature either. Examples of the pyroxene solvus at higher pressures, 5 to 15 kbar, are also furnished in the Lindsley (1983) address, but are derived from the 1-atm solvus and are not reviewed here except to say that the augite-pigeonite pairs also give linear partitioning results at pressure.

EXTENSION TO MULTI-COMPONENT SYSTEMS

At Figure 2 it was mentioned that linear plagioclase partitioning could be studied within such multi-component systems as anorthosite and gabbro. Experimental studies by Morse et al. (2004), McIntosh (2009), and Fram and Longhi (1992) all involved bulk compositions made up of natural mineral components. The liquid compositions for binary solutions within multi-component systems are obtained from the normative calculation of mineral components in quenched glass for which the composition is determined by electron probe. The norm calculations are commonly made in oxygen units and corrected for pyroxene compositions as found in nature rather than, for example, on the Di-Hd join at 50% wollastonite. Further details are reported by Morse et al. (2004). Extension to a global range of bulk compositions is reported in the study of large databases by Morse (2013), in which the problems and pitfalls of liquid calculations are discussed at some length. In what follows, the linear partitioning principle is extended to a suite of natural olivine compositions.

Always consult and cite the final, published document. See http://www.minsocam.org or GeoscienceWorld

KIGLAPAIT OLIVINE STUDIES

Here we begin with a review of olivine compositions in the entire intrusion (Morse, 1979a; 1996). Liquid compositions are then introduced from earlier-published estimates. Partitioning of augite against liquid and against olivine is reviewed with linear plots. The choice of exchange coefficient values is reviewed in the light of liquid structure as represented by NBO/T indices (where NBO is the sum of non-bridging oxygens and T is the number of tetrahedral cations: Mysen et al., 1982). Then the linear partitioning plots for olivine - liquid are examined. This exercise reveals a novel second linear array that identifies the liquid composition and might be used to deduce a previously existing liquid composition.

Stratigraphic relationships

Olivine compositions in the Kiglapait intrusion are plotted in stratigraphic context, Fig. 9, along with key arrivals of new phases augite, Fe-Ti oxide minerals, and apatite. The *X* axis is stratigraphic and runs from the base of the intrusion at the left to the top at the right. The PCS scale represents the volume percent solidified as calculated from cross sections (Morse, 1969). The logarithmic scale is based on the fraction of remaining liquid F_L, equal to 1-(PCS/100). It is used to display quantities in detail that would be simply a blur at linear scale.

The initial trend in the Lower Zone is limited in variation from Fo_{71} to about Fo_{61}. As shown also in Fig. 8 of Morse (2008) the expectation for cotectic olivine + plagioclase would be fractionation to Fo_{40} at 65 PCS. The retardation of the natural olivine variation in the Lower Zone can be attributed in considerable part to the evolving ferric iron component of the magma, which reduces the activity of the ferrous end-member fayalite. Much of the other scatter to high-Fo values, as found for example after 99.9 PCS, can also be attributed to the contact of olivine with grains of magnetite. Of note in the figure is the cluster of Fo-rich olivines labeled “Oxygen spikes” in the stratigraphic region after the Fe-Ti oxide minerals become important. The cause of the oxygen spikes was discussed in Morse (1979a,b) and particularly in Morse (1980) where the oxygen and silica activities of the magma were described in some detail. In that contribution,

Always consult and cite the final, published document. See http://www.minsocam.org or GeoscienceWorld

reversed rims on olivine grains among the titanomagnetite grains of the Main Ore Band were reported in Figure 4, ranging from $Fo_{58.8}$ to as high as Fo_{66}. A jump in f_{O2} from well below FMQ to well above FMQ at the top of the Main Ore Band was shown in figure 10 of that paper. This oxidation effect on local olivine compositions can be seen as a low-f_{O2} counterpart to the olivine hiatus in the Skaergaard intrusion, where the loss of olivine can be ascribed to a locally high silica activity that de-stabilizes Mg-olivine until the magma eventually evolves to a more iron-rich composition that stabilizes Fe-olivine (*e.g.*, Morse et al. 1980).

LIQUID COMPOSITIONS FOR KIGLAPAIT OLIVINE PARTITIONING

Kiglapait olivines and their parent liquids were discussed in detail by Morse (1996) and Morse (2001). The result for the Kiglapait liquid compositions in X_{Fe} = molecular $Fe^{2+}/(Fe^{2+}+Mg)$ was listed in Table 2 of he 1996 paper. These compositions were generated from the linear partitioning equation assuming $K_D = 0.33$ for all of the Lower Zone, 0-84 PCS, and varying to 0.45 at the end of crystallization based on earlier literature data. These assumptions are re-visited below.

Augite-Olivine relations

The linear partitioning of Kiglapait augite with liquid is demonstrated in Fig. 10a from data calculated from the QUILF equilibria with olivine and liquid (Morse, 1996). The solid-solid plot of augite on olivine compositions is shown in Fig. 10b in which three points lie well above the linear partitioning line defined by the other six points. This result was ascribed (Morse, 2001) to metastable, supercooled compositions of augite that crystallized early from augite-oversaturated liquids and became too Fe-rich as a result. [It might be thought that the olivines were at fault instead, being too Mg-rich, but the Mg-rich ("Ox-spikes") olivine compositions were not used in the cited paper.]

LIQUID POLYMERIZATION AND OLIVINE PARTITIONING

Experimental and theoretical investigation has shown that the partitioning of olivine and

Always consult and cite the final, published document. See http://www.minsocam.org or GeoscienceWorld

379 silicate melts clearly depends on the polymerization of the melt. Among significant steps in the
380 evolution of this principle are studies by Kushiro and Walter (1998), Toplis (2004), and Mysen
381 (2007). The NBO/T data[2] for experimental Kiglapait liquid compositions (Fig. 11) show a base
382 line near a value 0.8, increasing to > 1.0 near the augite + oxide mineral maximum, and with a
383 long gap to ~1.0 in the Upper Zone. Very mafic samples have high values of NBO/T, as seen in
384 three cases at 95 and ~99.9 PCS. All other liquid samples plot among those for the rocks, so the
385 paucity of data for liquids between 93 and 99.7 PCS is of little concern. This range in NBO/T lies
386 essentially at the crest of Mysen's (2007) figure 7 where the values of K_D range from ~0.23 to
387 0.35, with a mean of 0.27. A formal calculation with a best fit to the experimental data can be
388 made as follows. Using a best fit for the experimental data represented by the gray filled circles in
389 Fig. 11, we have a stratigraphic variation of NBO/T, as follows. For x = the stratigraphic measure
390 "-log F_L", NBO/T (experimental) = $-.0614x^2 + 0.2811x + 0.6452$. From this and the diagram of
391 K_D v. NBO/T of Mysen's (2007) figure 7 we solve for K_D as follows: For x = NBO/T, $K_D = 0.01x^3$
392 $- 0.1053x^2 + 0.2118x + 0.155$. The values of K_D vary from 0.25 to 0.27, with a mean of 0.26.
393 These values are significantly lower than previously assumed to be ≥ 0.33.

394 From these results we can now generate a new estimate of the liquid composition in
395 equilibrium with the observed olivine compositions in the Kiglapait intrusion. The result is shown
396 in Fig. 12.

397 ## LINEAR PARTITIONING OF OLIVINE IN THE KIGLAPAIT INTRUSION

398 **Region 50 PCS to the end of crystallization**

399 The partitioning result for the whole intrusion is shown in Fig. 13, where the derived criterion
400 of the mean value of $K_D = 0.26$ is identified by a horizontal line. The data for all stratigraphic
401 levels above 50 PCS are shown as black filled circles. The data are partly from the Lower Zone,
402 50-84 PCS, and the rest are from the Upper Zone, >84 PCS. The previously noted "oxygen

[2]Calculations of NBO/T for this contribution were made in a spreadsheet kindly furnished by B. O. Mysen.

Always consult and cite the final, published document. See http://www.minsocam.org or GeoscienceWorld

spikes" from Fig. 9 are clearly revealed in this linear partitioning plot. The scatter of data about the nominal trend line is to a lesser extent due to the small variation of K_D values ± 0.01 from the mean of 0.26, and to greater extent due to local variations in crystal nucleation and growth, and the subsequent effects of trapped liquid.

Lower Zone 0-50 PCS

The data plotted in gray filled circles occupy a completely different trend in the linear partitioning diagram. The trend originates precisely at the origin (1, 0). The crystal compositions are measured and therefore unquestioned. These samples do not plot as expected for reasons discussed below. This array is the graphical solution to the problem of finding the liquid composition at the $y = 1.0$ intercept, given the crystal composition and the value of K_D. The novel array has the equation $y = -ax + a$, where $a \geq 1.0$ is a function of slope, as shown near the base of Fig. 13.

INTERPRETATIONS OF THE NOVEL ARRAY

It is essential here to recapitulate the origin of the partitioning arrays and particularly the new array. The crystal compositions are measured in grain mounts and represent secure input data. The liquid compositions are calculated from the crystal compositions using the linear partitioning equation and the experimental values of NBO/T and K_D. It is of interest that the upper intercept value of the new array at $D = 1.0$ does reliably represent the liquid composition in equilibrium with the nominal maximum crystal composition at Fo_{71}. This fact demonstrates internal consistency, given the value of K_D used. It is also to be noted that the lower values of K_D now used, based on the experimental NBO/T, are lower than the Roeder-Emslie result and they consequently describe a fatter loop than that shown in Fig. 1a (but not as fat as that in Fig. 1b).

There are at least three plausible origins for the new array. It could represent equilibrium crystallization in which cumulus olivine crystals have reacted with intercumulus (trapped) liquid

Always consult and cite the final, published document. See http://www.minsocam.org or GeoscienceWorld

having the composition of the main magma. Or it could represent partial quenching of magma in a chilled margin in which liquids were to variable extent supercooled to the solidus. Or it could represent a mistaken assumption that the liquid producing the new array was that of the main magma, whereas it was in fact a magma with a more evolved composition.

These multiple working hypotheses can be tested in various ways. The first is to test the evidence from plagioclase. The next is to test the stratigraphic relationships of the samples in the array. Another is to find a calculation of some assumed quantity that makes the new array disappear. All three of these tests are in progress, and the final result will be reported in a separate contribution. It can be anticipated that some degree of each cause could play a role, but that one central principle will be dominant. The equilibrium crystallization hypothesis is mostly falsified by the plagioclase data and the lack of correlation with measured trapped liquid volumes. The extent of the array to half the entire volume of the Kiglapait magma makes the quenching notion seem unlikely. It remains to test and document the extent and effect of the liquid composition, and to find the least ambiguous result.

IMPLICATIONS

The study of linear partitioning and its systematics leads to new questions and answers about old rocks – the ones we see that crystallized in the past. It is a tool that allows the observer to calculate a magma composition from the crystal composition. Although mathematical and simple, it leads into serious considerations about unknown mixing properties of melts and crystals. It presents the following dilemma. In azeotropic systems such as Albite-Orthoclase where two loops meet in a conjugate minimum, we know very well the non-ideality of the solutions (solid and liquid). And yet the linear partitioning arrays are rigorously straight. So linear partitioning in such cases reveals nothing about the non-ideality of the liquid. Without the azeotropic constraint, some systems also show rigorously straight linearity, whilst other systems require curved or segmented partitioning arrays. The plagioclase feldspars are a case in point: they clearly form a true binary loop, but give curved partitioning. Better enthalpy data than used here are required, but the true meaning of the curve must be a target for future enlightenment about the interaction of the mixing

Always consult and cite the final, published document. See http://www.minsocam.org or GeoscienceWorld

454 properties of solutions. The one should predict the other. These are classic systems known and
455 studied for 102 years and yet still full of secrets. The novel partitioning array could have
456 important consequences for understanding the history of mafic intrusions.

457 ## ACKNOWLEDGMENTS

458 I am grateful for the comments by an anonymous reviewer that led to correction of some
459 significant problems in the manuscript. The intensive review and commentary by Associate Editor
460 Bjorn Mysen were extremely helpful and resulted in many improvements and corrections.
461 Further intensive attentions by the Editor, Keith Putirka, are gratefully acknowledged. This article
462 is based on research supported by NSF under Award No. 0948095.

463 ## REFERENCES CITED

464 Andersen, D.J., Lindsley, D.H., and Davidson, P.M. (1993) QUILF: a Pascal program to assess
465 equilibria among Fe-Mg-Mn-Ti oxides, pyroxenes, olivines, and quartz. Computers and
466 Geosciences 9, 1333-1350.

467 Anovitz, L.M., and Blencoe, J.G. (1999) Dry melting of albite. American Mineralogist 84,
468 1830-1842.

469 Beattie, P., Drake, M., Jones, J., Leeman, W., Longhi, J., McKay, G., Nielsen, R., Shaw, D.,
470 Takahashi, E., and Watson, B. (1993), Terminology for trace-element partitioning.
471 Geochimica et Cosmochimica Acta, 57, 1605-1606.

472 Bowen, N.L. (1913) The melting phenomena of the plagioclase feldspars. American Journal of
473 Science 25, 577-599.

474 Bowen, N.L. (1915) The crystallization of haplobasaltic, haplodioritic, and related magmas.
475 American Journal of Science, 40, 161-185.

Always consult and cite the final, published document. See http://www.minsocam.org or GeoscienceWorld

Bowen, N.L., and Schairer J.F. (1935) The system, MgO-FeO-SiO_2. American Journal of Science 5th Series, 29, 151-217.

Bradley, R. S. (1962) Thermodynamic calculations on phase equilibria involving fused salts. Part II. Solid solutions and application to the olivines. American Journal of Science, 260, 550-554.

Fram, M.S., and Longhi, John (1992) Phase equilibria of dikes associated with Proterozoic anorthosite complexes. American Mineralogist, 77, 605-616.

Hoover, J.D., and Irvine, T.N. (1978) Liquidus phase relations and Mg-Fe partitioning on part of the system Mg_2SiO_4 - Fe_2SiO_4- $CaMgSi_2O_6$ - $KAlSi_3O_8$ - SiO_2. Carnegie Institution of Washington Year Book 77, 774-784.

Kushiro, Ikuo (1973) The system diopside-anorthite-albite: determination of compositions of coexisting phases. Carnegie Institution of Washington Year Book 72, 502-507.

Kushiro, Ikuo, and Walter, M. J. (1998) Mg-Fe partitioning between olivine and mafic-ultramafic melts. Geophysical Research Letters 25, 2337-2340.

van Laar, J. J. (1908) Die Schmelz- oder Erstarungskurven bei binären Systemen, wenn die feste Phase ein Gemisch (amorphe feste Lösung oder Mischkrystall) der beiden Komponenten ist. Zeitschrift Physikalische Chemie, 64, 257-297. *[The melting- or evaporation-curve of binary systems, when the condensed phase is a mixture (amorphous condensed solution or mix-crystal) of both components. – SAM]*.

Lange, R.A. (2003) The fusion curve of albite and the compressibility of $NaAlSi_3O_8$ liquid with pressure. American Mineralogist, 88, 109-120.

McIntosh, D.B. (2009) High pressure liquidus studies of the inferred magma composition of the Kiglapait layered intrusion, Labrador, Canada. MS thesis, University of Massachusetts.

Lindsley, D.H. (1983) Pyroxene thermometry. American Mineralogist, 68, 477-493.

Morse, S. A. (1969) *The Kiglapait Layered Intrusion, Labrador.* Geological Society of America

Always consult and cite the final, published document. See http://www.minsocam.org or GeoscienceWorld

501 Memoir 112, 204 pp.

502 Morse, S.A. (1970) Alkali feldspars with water at 5 kb pressure. Journal of Petrology, 11, 221-
503 251.

504 Morse, S.A. (1979a) Kiglapait geochemistry I: Systematics, sampling, and density. Journal of
505 Petrology, 20, 555-591.

506 Morse, S.A. (1979b) Kiglapait geochemistry II: Petrography. Journal of Petrology, 20, 592-624.

507 Morse, S.A. (1980) Kiglapait mineralogy II: Fe-Ti oxide minerals and the activities of oxygen and
508 silica. Journal of Petrology, 21, 685-719.

509 Morse, S.A. (1981) Kiglapait geochemistry IV: The major elements. Geochimica et Cosmochim
510 Acta, 45, 461- 479.

511 Morse, S.A. (1994) Basalts and Phase Diagrams. Corrected and reprinted by Krieger, Melbourne,
512 FL, 493 pp.

513 Morse, S.A. (1996) Kiglapait mineralogy III: Olivine compositions and Rayleigh fractionation
514 models. Journal of Petrology, 37, 1037-1061.

515 Morse, S.A. (1997) Binary solutions and the lever rule revisited. Journal of Geology 105, 471-
516 482.

517 Morse, S.A. (2000) Linear partitioning in binary solutions. Geochimica et Cosmochimica
518 Acta,64, 2309-2319.

519 Morse, S.A. (2001) Augite-olivine equilibria in the Kiglapait Intrusion, Labrador, Canada.
520 Canadian Mineralogist, 39, 267-274.

521 Morse, S.A. (2008) The internal magma reservoir of large intrusions revealed by multiphase
522 Rayleigh fractionation. Journal of Petrology, 49**,** 2081-2098.

523 Morse, S.A. (2012) Plagioclase An range and residual porosity in igneous cumulates of the
524 Kiglapait Intrusion. Journal of Petrology, 53, 891-918.

Always consult and cite the final, published document. See http://www.minsocam.org or GeoscienceWorld

525 Morse, S.A. (2013) Experimental equilibrium tested by plagioclase loop widths. Journal of
526 Petrology, 54, 1793-1813.

527 Morse, S. A., and Ross, Malcolm (2004). Kiglapait mineralogy IV: The augite series. American
528 Mineralogist, 89, 1380-1395.

529 Morse, S.A., Brady, J.B., and Sporleder, B.A. (2004) Experimental petrology of the Kiglapait
530 intrusion: Cotectic trace for the Lower Zone at 5kb in graphite. Journal of Petrology, 45,
531 2225-2259.

532 Morse, S.A., Lindsley D.H, and Williams R.J. (1980) Concerning intensive parameters in the
533 Skaergaard intrusion. American Journal of Science, 280-A (Jackson Vol.),159-170.

534 Mysen, B.O. (2007) Partitioning of calcium, magnesium, and transition metals between olivine
535 and melt governed by the structure of the silicate melt at ambient pressure. American
536 Mineralogist 92, 844-862.

537 Mysen, B.O., and Richet, P. (2005) Silicate Glasses and Melts - Properties and Structure.
538 Developments in Geochemistry, New York: Elsevier, 548 pp.

539 Mysen, B.O., Virgo, D. and Seifert, F.A. (1982) The structure of silicate melts: Implications for
540 chemical and physical properties of natural magma. Reviews of Geophysics and Space
541 Physics, 20, 353-383.

542 Navrotsky, A., Hon, R., Weill, D.F., and Henry, D.J. (1980) Thermochemistry of glasses and
543 liquids in the systems $CaMgSi_2O_6$-$CaAl_2Si_2O_8$-$NaAlSi_3O_8$, SiO_2-$CaAl_2Si_2O_8$-$NaAlSi_3O_8$ and
544 SiO_2-Al_2O_3-CaO-Na_2O. Geochimica et Cosmochimica Acta, 44, 1409-1413.

545 Nekvasil, H. (1992) Feldspar crystallization in felsic magmas: A review. Transactions Royal
546 Society Edinburgh Earth Science, 83, 399-407.

547 Osborn, E.F. (1942) The system $CaSiO_3$ - diopside - anorthite. American Journal of Science 240,
548 751-788.

549 Peterson, A.L. (1999) Quest for the liquid line of descent of the Upper Zone of the Kiglapait

Always consult and cite the final, published document. See http://www.minsocam.org or GeoscienceWorld

intrusion, Labrador, Canada: an experimental study. MS thesis, University of Massachusetts, 80 pp.

Ramberg, H. (1952) The Origin of Metamorphic and Metasomatic Rocks. Chicago University Press, Chicago.

Richet, P., and Bottinga, Y. (1986) Thermochemical properties of silicate glasses and liquids: A review. Reviews in Geophysics, 24, 1-25.

Robie, R.A., Hemingway, B.S., and Fisher, J.R. (1978) Thermodynamic properties of minerals and related substances at 298.15 K and 1 bar (10^5 Pascals) pressure and at higher temperatures. Washington, DC: US Government Printing Office, Geological Survey Bulletin No. 1452.

Roeder, P.L., and Emslie, R.F. (1970) Olivine-liquid equilibrium. Contributions to Mineralogy and Petrology, 29, 275-289.

Schairer, J.F., and Bowen, N.L. (1956) The system Na_2O - Al_2O_3 - SiO_2. American Journal of Science 254, 681-746.

Toplis, M.J. (2005) The thermodynamics of iron and magnesium partitioning between olivine and liquid: criteria for assessing and predicting equilibrium in natural and experimental systems. Contributions to Mineralogy and Petrology, 149, 22-39.

Waldbaum, D.R. (1969) Thermodynamic mixing properties of NaCl - KCl liquids. Geochimica et Cosmochimica Acta, 33, 1415-1427.

Waldbaum, D.R., and Thompson, J.B. Jr. (1969) Mixing properties of sanidine crystalline solutions. IV. Phase diagrams from equations of state. American Mineralogist, 54, 1274-1298.

Weishaupt, J. (1975) Thermodynamic Equilibria of Boiling Mixtures. Landholt-Börnstein, New Ser. Gp. IV. 3. Springer-Verlag, Berlin.

Always consult and cite the final, published document. See http://www.minsocam.org or GeoscienceWorld

FIGURE CAPTIONS

Fig. 1. (a) Components of a linear partitioning diagram using the olivine melting series Fo-Fa as an example. Symbols: *D,* partition coefficient; *X*, mole fraction; K_D, exchange coefficient with value from Roeder and Emslie (1970); (S), solid; (L), liquid; Fa, fayalite (Fe end member); Fo, forsterite (Mg end member). (b) With the value of K_D changed to 0.2, for values of NBO/T equal to either 0.2 or 2.4, from a concave-down relationship of K_D with NBO/T illustrated by Mysen (2007). This figure illustrates the inverse relationship between K_D and loop width.

Fig. 2. Characteristics of binary loops related to linear partitioning. Symbols: An, anorthite content in percent = 100 X_{An}, $X_2 = X_{An}$. (a) Variation of loop width with for varying values of K_D with a fixed crystal composition of An_{60}. The curve is calculated from a spreadsheet that generates *T-X* loops for differing values of K_D. (b) The pressure effect on natural plagioclase feldspar. Fram and Longhi (1992) found that a natural anorthosite showed an increase of K_D with pressure up to 27 kbar, and a gabbroic composition showed a steeper correlation. With the work of Morse et al. (2004) and McIntosh (2009) the combined data show a strong pressure effect yielding the relationship shown in the figure. See also Fig. 7 of Morse (2013) for more details.

Fig. 3. Linear partitioning diagram for the boiling mixture Methylcyclohexane ("MCH") - CCl4 with data taken from Weishaupt (1975). The ordinate is the partition coefficient for the mole fraction of CCl4 in the liquid (L) divided by that in the vapor (V).

Fig. 4. Linear partitioning diagram for the boiling mixture CCl4-Acetone. The data curve fails the linear test. Inset: *T-X* loop for the system.

Fig. 5. The azeotropic melting diagram for sanidine crystalline solutions, the system Ab-Or. A. The *T-X* diagram; AP = the azeotropic point. The Or-rich liquidus is metastable with respect to leucite plus liquid because of the incongruent melting of sanidine. The temperatures are

Always consult and cite the final, published document. See http://www.minsocam.org or GeoscienceWorld

596 uncorrected for the adjustment to 1100 °C for albite melting (Anovitz & Blencoe, 1999). The
597 binary loops are plotted from the data in Table 2 of Waldbaum and Thompson (1969). B. the
598 linear partitioning diagram constructed from regressions on the same table, along with the
599 isotherms. The individual AP intercepts of the regression are listed near the top of the diagram,
600 and their average is given as the AP at $X_{Or} = 0.331$. The regressions are described by the two
601 equations with adjustments as described in the text.

602 Fig. 6. The system Di-An-Ab. A. The *T-X* loop calculated from the linear regression shown in
603 (B). The inset shows the ternary phase diagram with cotectic. B. The linear regression, re-plotted
604 from Morse (1997).

605 Fig. 7. The system An-Ab. A. The *T-X* diagram recalculated in Bowen's method from the new
606 enthalpies of fusion as described in the text. B. The linear partitioning result. The dotted array
607 with a kink at An_{60} is calculated using the original latent heat ΔH_f (An) from Bowen. The solid
608 curve is the result of using a newer value of that enthalpy, from Navrotsky et al. (1980), with the
609 second-order polynomial fit shown. The similarity between the two curves recalls Bowen's error
610 analysis, in which errors in latent heat can result in excessive errors in temperature.

611 Fig. 8. Two pairs of solutions from the pyroxene quadrangle (Lindsley, 1983). A. Augite-
612 Pigeonite with an exact received intercept at 1.00 and a K_D value of 0.74. B. Augite-
613 Orthopyroxene, with no linear partitioning.

614 Fig. 9. Kiglapait olivine compositions in stratigraphic context. The "oxygen spikes" refer to
615 stratigraphically abnormal Mg-rich samples associated with titanomagnetite crystals that reflect
616 enhanced ferric iron in the melt, thereby depleting the local activity of the ferrous component in
617 the olivine. This matter is discussed at some length in the text. Symbols: MOB, Main Ore Band;
618 Aug, augite; Ox, titanomagnetite; Ap, apatite; PCS, volume percent solidified; *F*(L) fraction of
619 system present as liquid.

Always consult and cite the final, published document. See http://www.minsocam.org or GeoscienceWorld

Fig. 10. Kiglapait augite-olivine-liquid relations in linear partitioning diagrams, calculated from olivine compositions and QUILF equilibria. (a) Augite-liquid partitioning with $K_D = 0.19$ (Morse and Ross, 2004). (b) Augite-olivine equilibria simplified from Morse (2001) showing the off-line results for early augites interpreted in the cited study as being metastable.

Fig. 11. Calculated ratios of non-bridging oxygens divided by tetrahedral cations (NBO/T; *e.g.*, Mysen and Richet, 2005) for Kiglapait whole rocks (solid black diamonds) and experimental liquids (quenched melts, in grayscale,) for the Lower Zone (Morse et al. 2004) and the uppermost Upper Zone (Peterson, 1999). Note that feldspar-rich, hence more polymerized, compositions (in the Lower Zone and above 95 PCS) have *low* values of NBO/T, whereas feldspar-poor compositions rich in mafic minerals have *higher* values. Whole-rock analyses are from Morse (1981). The curve for the whole-rocks accurately reflects the arrival and over-production of augite and Fe-Ti oxide minerals in the region 85-95 PCS (modal data from Morse, 1979b). The sag after 95 PCS reflects a local increase and maximum in the amount of normative feldspar, as does the tail-end of the data at the end of crystallization. Two high values near 99.9 PCS are low-silica, mafic compositions with only 40-44 % normative feldspar and 57- 60 % normative augite + olivine. Otherwise, most of the liquid compositions are similar to the whole-rock compositions. Abbreviation: OG, olivine gabbro. The data for the liquids help to define the more appropriate value of K_D for olivine-liquid equilibria.

Fig. 12. Estimated X_{Fe} compositions of Kiglapait liquids, derived from Fig. 11, transformed as described in the text. The stratigraphically varying value of K_D is applied to the crystal compositions to find the value of X_{Fe}^{L} from the linear partitioning equation.

Fig. 13. Linear partitioning plot of all Kiglapait olivine compositions, for which the liquid compositions are those from Fig. 12. The horizontal line identifies the mean value of the exchange coefficient as $K_D = 0.26$. The black data points reflect all data above 50 PCS, including points from the Lower Zone 50-84 PCS and all the data from the Upper Zone, defined as >84 PCS. The

Always consult and cite the final, published document. See http://www.minsocam.org or GeoscienceWorld

gray filled circles represent all the data from 0 to 50 PCS. These points define a novel array arising from the lower right corner of the diagram with the dotted line and equation shown. The upper intercept of this regression gives the value of the initial liquid composition assumed for the earliest crystals with Fo ~ 71. The origin of this array has three possible causes, as discussed in the text. The two most likely are an initial evolved magma and the effects of early trapped liquid.

Always consult and cite the final, published document. See http://www.minsocam.org or GeoscienceWorld

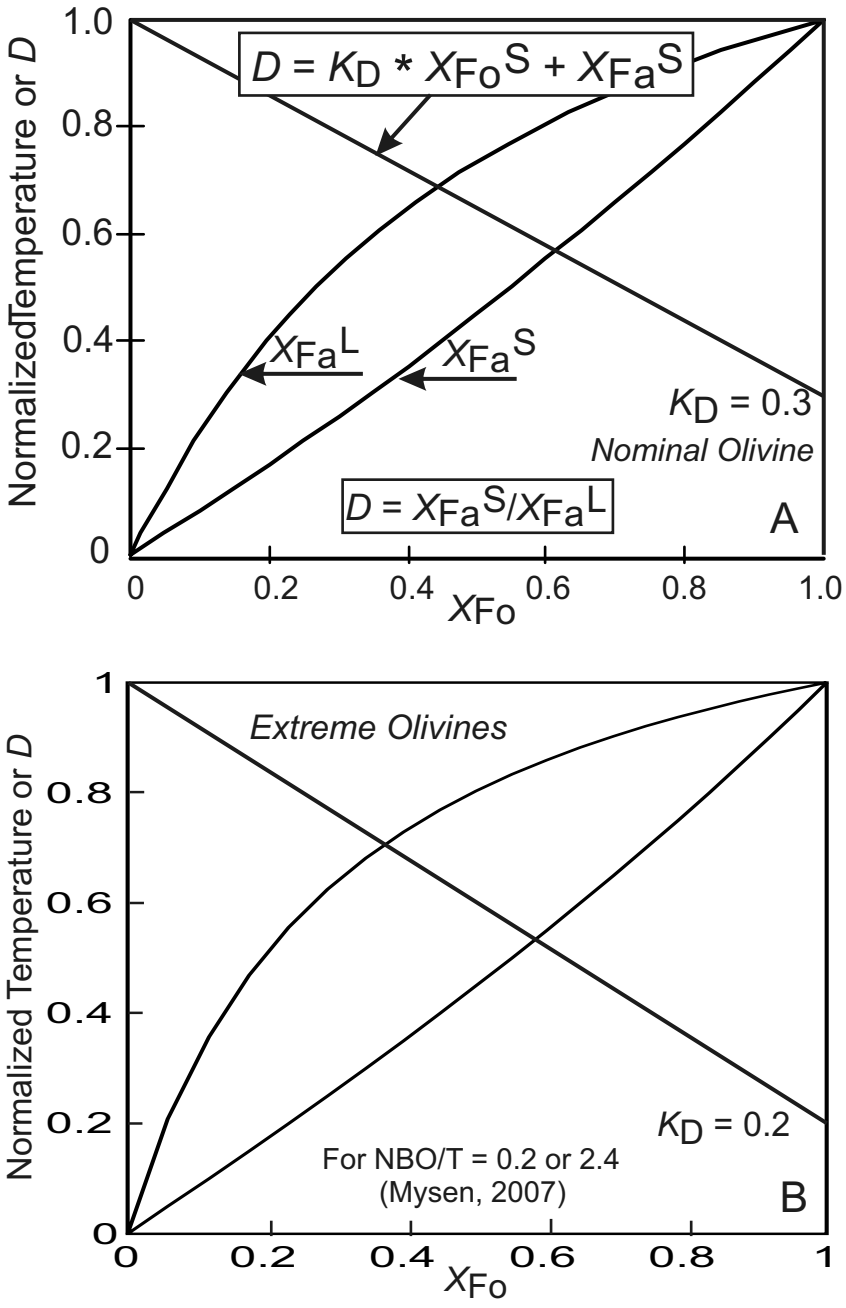

Morse Figure 1

This is a preprint, the final version is subject to change, of the American Mineralogist (MSA)
Cite as Authors (Year) Title. American Mineralogist, in press.
(DOI will not work until issue is live.) DOI: http://dx.doi.org/10.2138/am-2015-5056

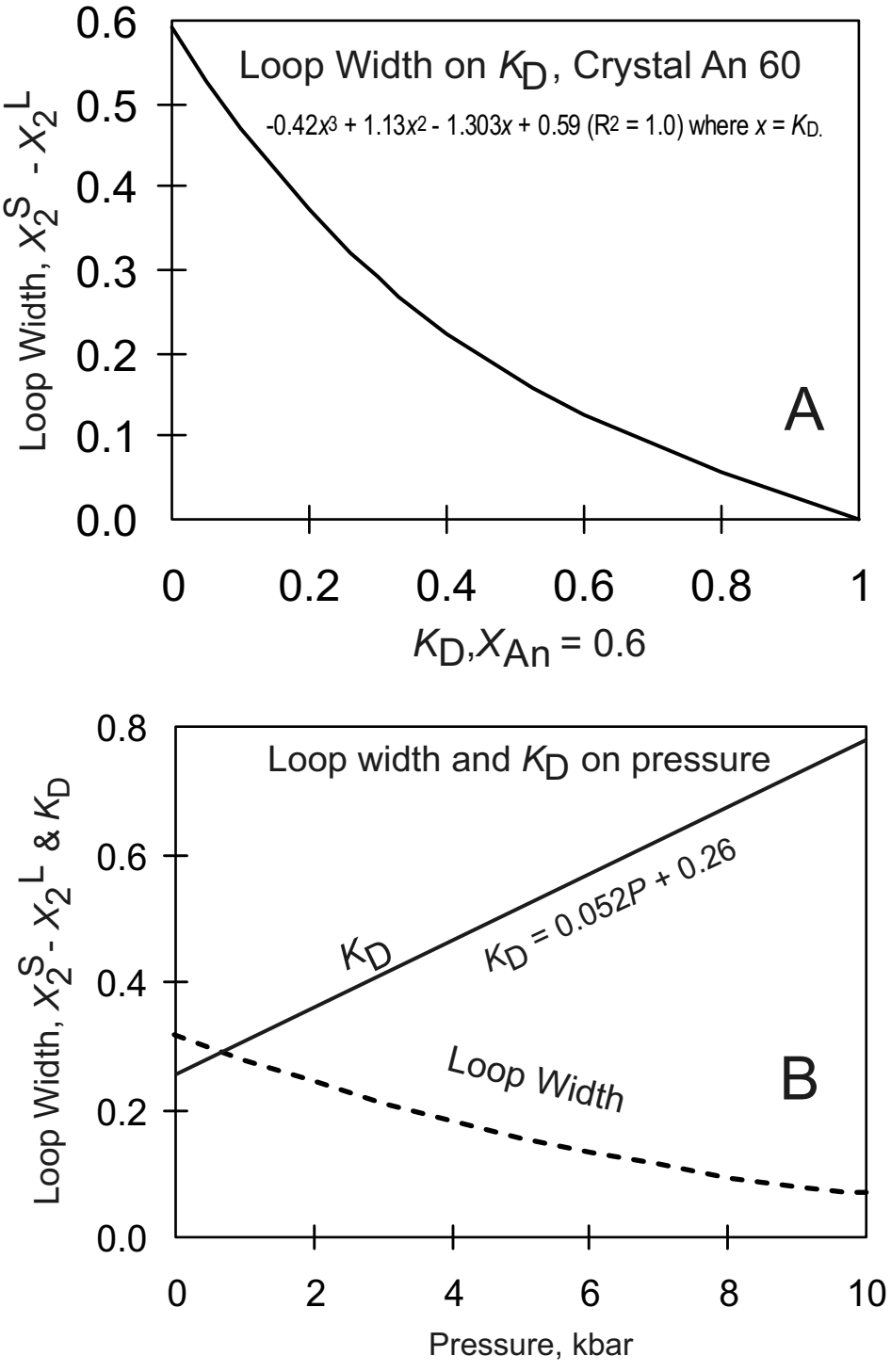

Morse Fig. 2

Always consult and cite the final, published document. See http://www.minsocam.org or GeoscienceWorld

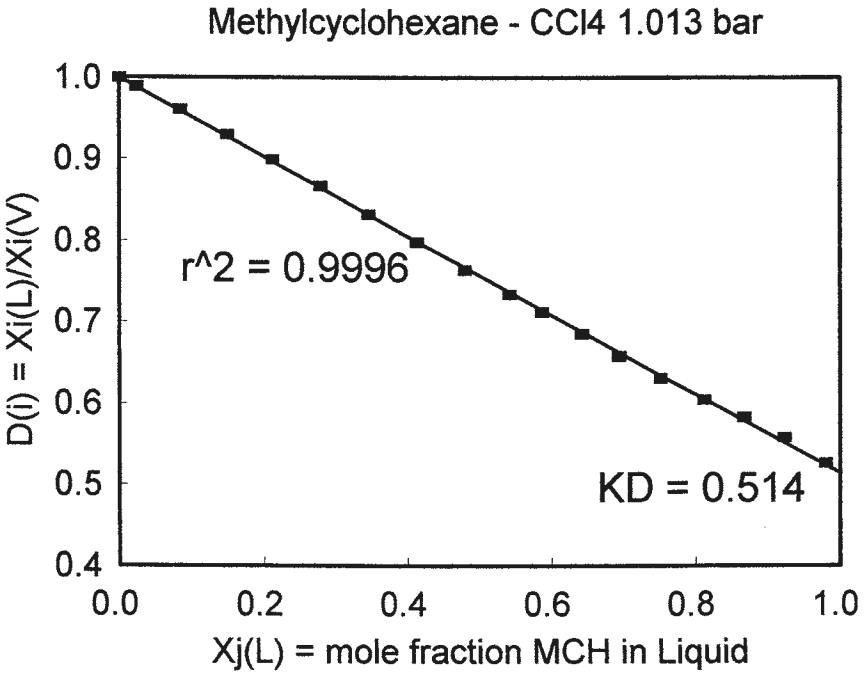

Meth ccl4

Morse Fig. 3

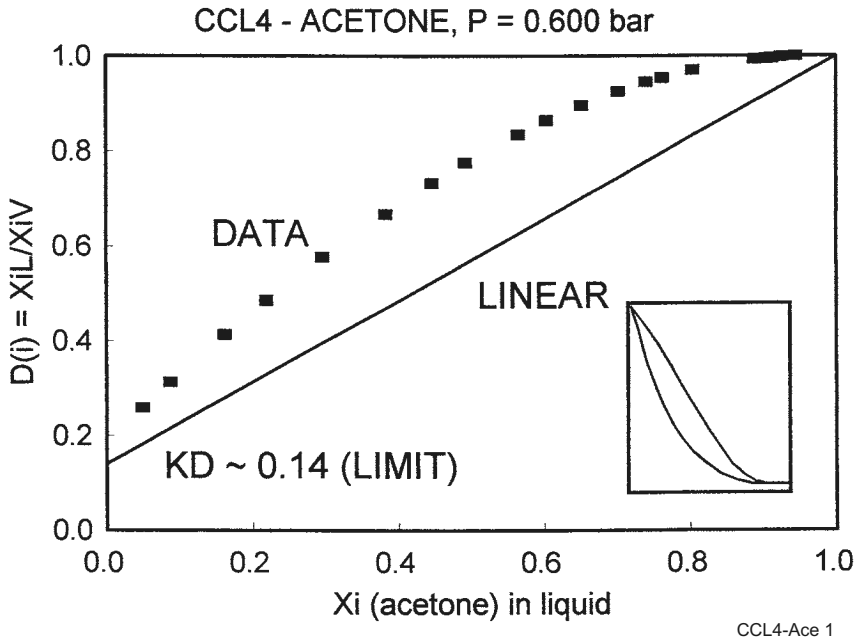
CCL4 - ACETONE, P = 0.600 bar
D(i) = XiL/XiV
1.0
0.8
0.6
0.4
0.2
0.0
DATA
LINEAR
KD ~ 0.14 (LIMIT)
0.0
0.2
0.4
0.6
0.8
1.0
Xi (acetone) in liquid
CCL4-Ace 1

Morse Fig. 4

eprint, the final version is subject to change, of the American Mineral
Cite as Authors (Year) Title. American Mineralogist, in press.
ill not work until issue is live.) DOI: http://dx.doi.org/10.2138/am-201

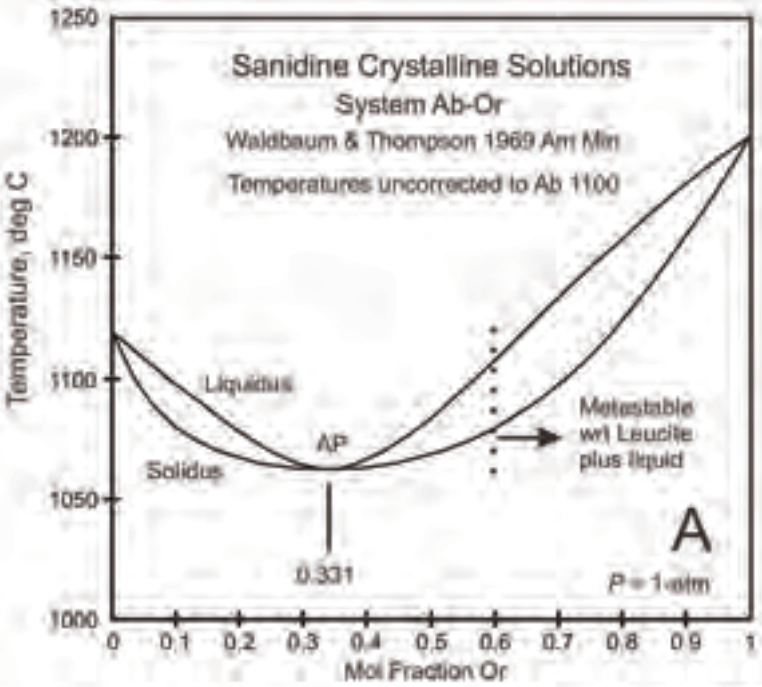

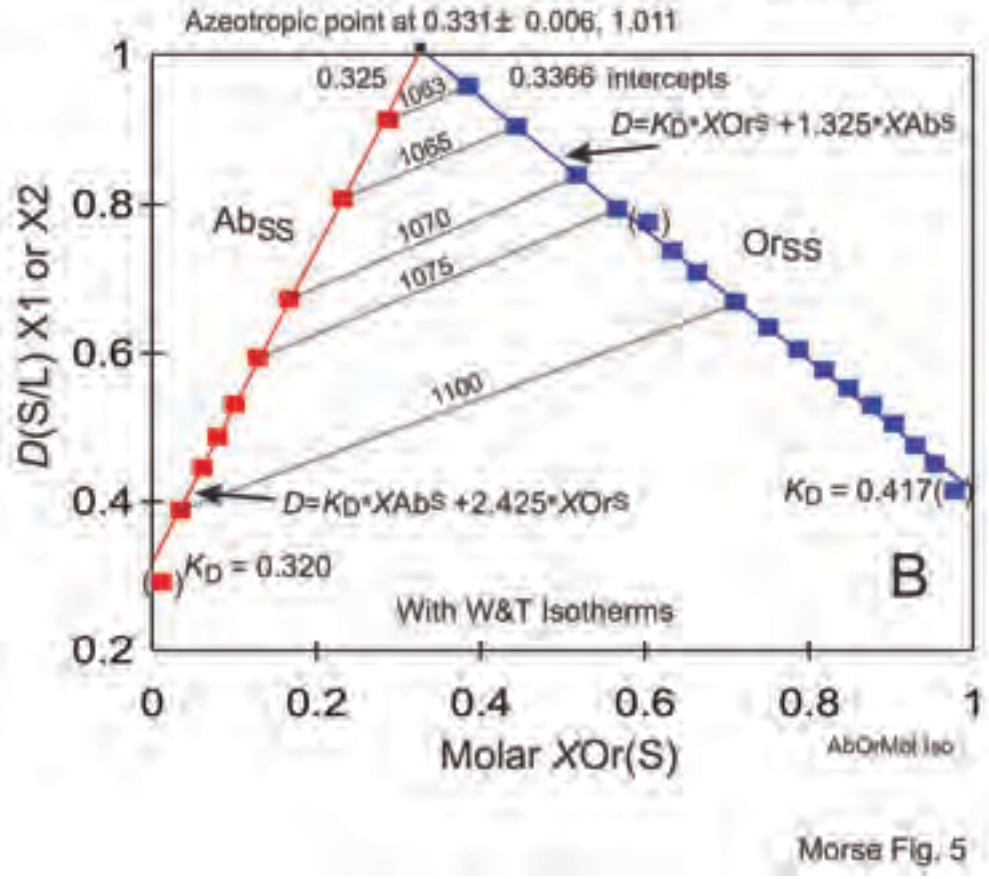

Morse Fig. 5

l cite the final, published document. See http://www.minsocam.org o

This is a preprint, the final version is subject to change, of the American Mineralogist (MSA)
Cite as Authors (Year) Title. American Mineralogist, in press.
(DOI will not work until issue is live.) DOI: http://dx.doi.org/10.2138/am-2015-5056

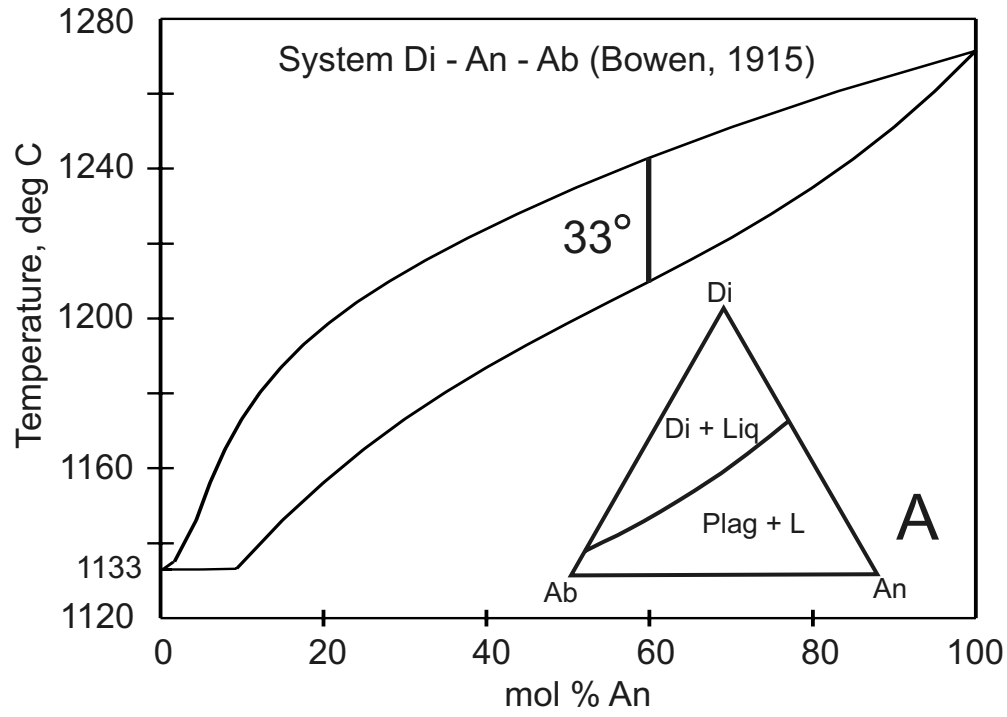

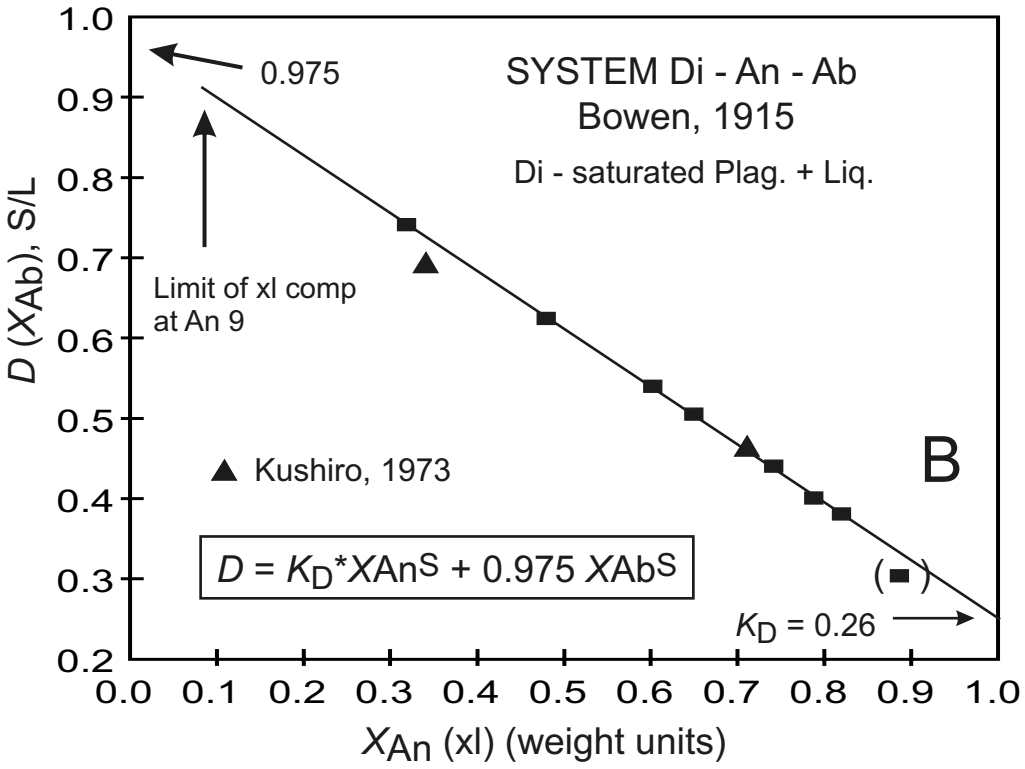

DAnAb 14

DiAnAb TX 15

Morse Fig. 6

Always consult and cite the final, published document. See http://www.minsocam.org or GeoscienceWorld

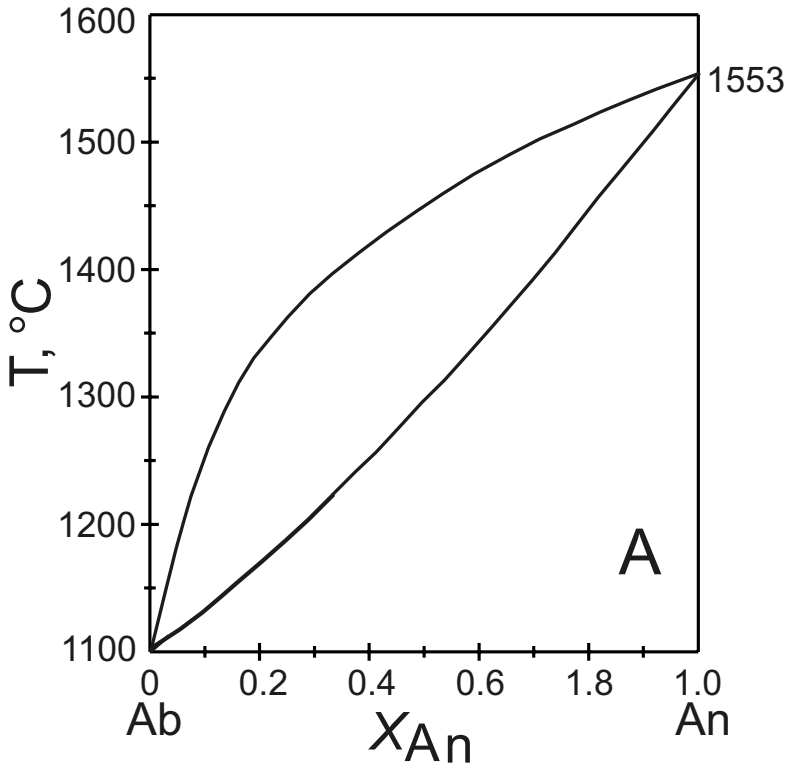
1600
1500
1400
1300
1200
1100
T, °C
1553
A
0
0.2
0.4
0.6
1.8
1.0
Ab
An
X_{An}

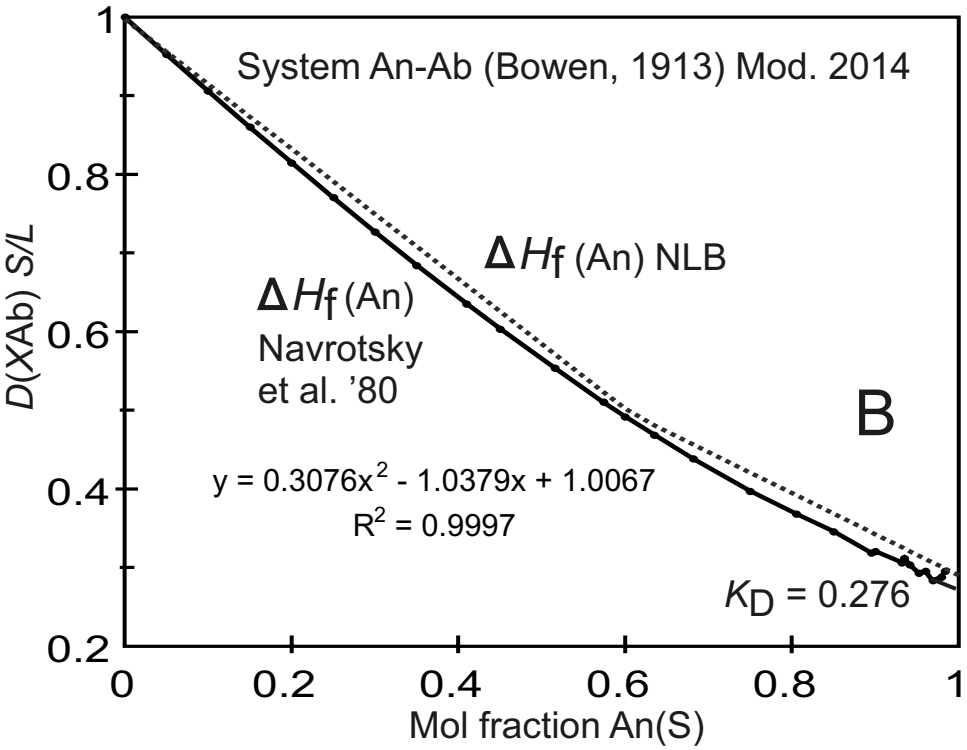
System An-Ab (Bowen, 1913) Mod. 2014
ΔH_f (An) NLB
ΔH_f (An)
Navrotsky
et al. '80
B
y = 0.3076x^2 - 1.0379x + 1.0067
R^2 = 0.9997
K_D = 0.276
D(XAb) S/L
1
0.8
0.6
0.4
0.2
0
0.2
0.4
0.6
0.8
1
Mol fraction An(S)

Morse Fig. 7

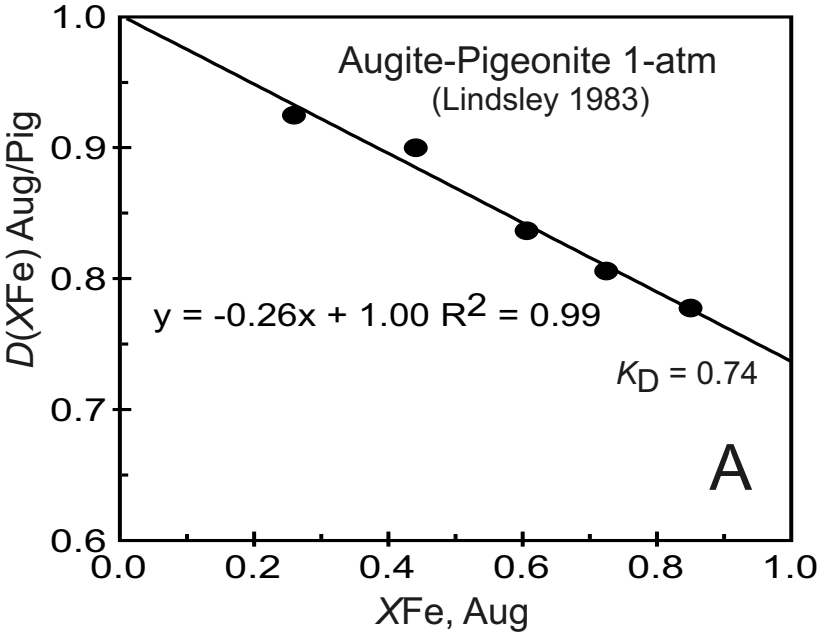
Augite-Pigeonite 1-atm
(Lindsley 1983)
y = -0.26x + 1.00 R2 = 0.99
KD = 0.74
A
D(XFe) Aug/Pig
XFe, Aug
1.0
0.9
0.8
0.7
0.6
0.0
0.2
0.4
0.6
0.8
1.0

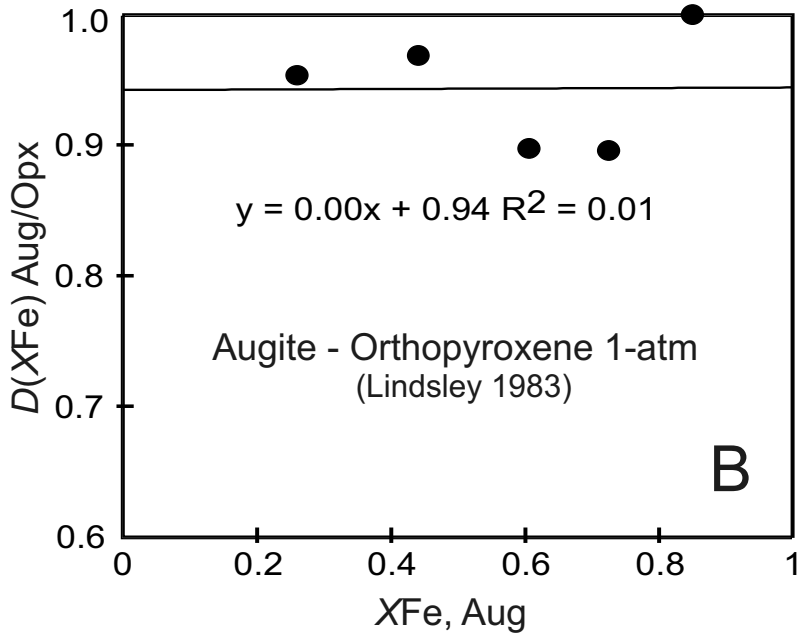
y = 0.00x + 0.94 R2 = 0.01
Augite - Orthopyroxene 1-atm
(Lindsley 1983)
B
D(XFe) Aug/Opx
XFe, Aug
1.0
0.9
0.8
0.7
0.6
0
0.2
0.4
0.6
0.8
1

Morse Fig. 8

This is a preprint, the final version is subject to change, of the American Mineralogist (MSA)
Cite as Authors (Year) Title. American Mineralogist, in press.
(DOI will not work until issue is live.) DOI: http://dx.doi.org/10.2138/am-2015-5056

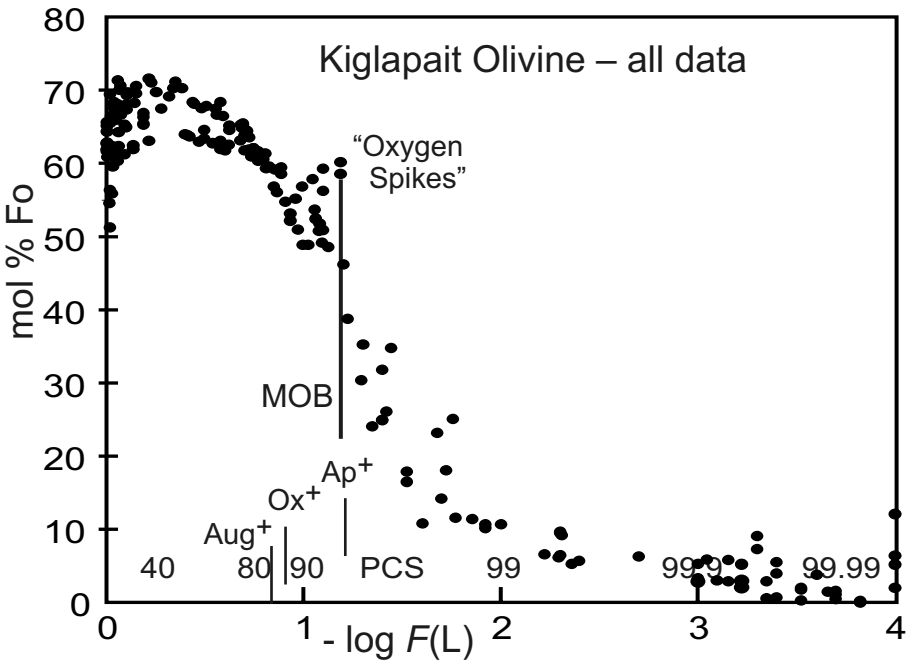

OL FO All 14

Morse Fig. 9

Always consult and cite the final, published document. See http://www.minsocam.org or GeoscienceWorld

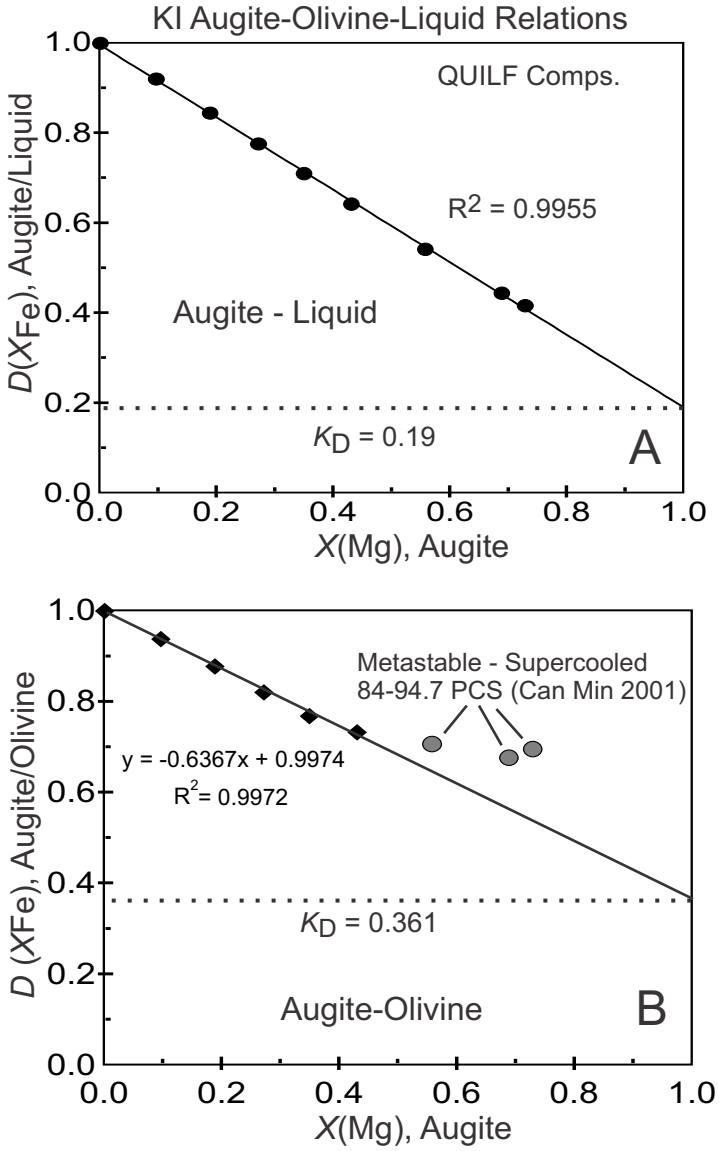
KI Augite-Olivine-Liquid Relations
QUILF Comps.
R^2 = 0.9955
Augite - Liquid
K_D = 0.19
A
$D(X_{Fe})$, Augite/Liquid
X(Mg), Augite
Metastable - Supercooled
84-94.7 PCS (Can Min 2001)
y = -0.6367x + 0.9974
R^2= 0.9972
K_D = 0.361
Augite-Olivine
B
D (XFe), Augite/Olivine
X(Mg), Augite

Morse Fig. 10

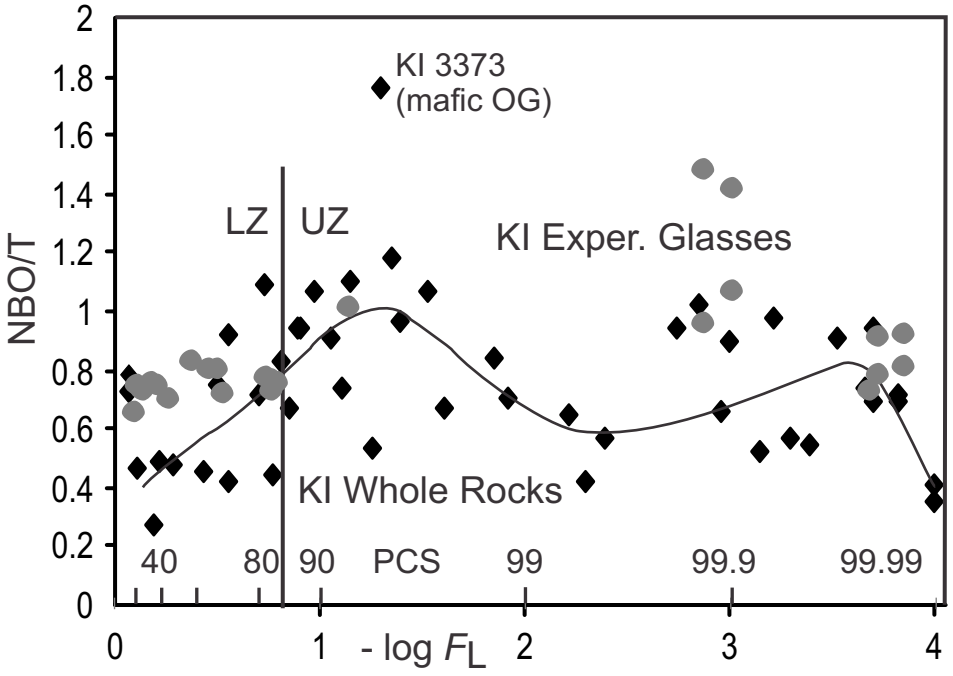
NBO/T
2
1.8
1.6
1.4
1.2
1
0.8
0.6
0.4
0.2
0
KI 3373
(mafic OG)
LZ
UZ
KI Exper. Glasses
KI Whole Rocks
40
80
90
PCS
99
99.9
99.99
0
1
- log F_L
2
3
4

Morse Fig. 11

This is a preprint, the final version is subject to change, of the American Mineralogist (MSA)
Cite as Authors (Year) Title. American Mineralogist, in press.
(DOI will not work until issue is live.) DOI: http://dx.doi.org/10.2138/am-2015-5056

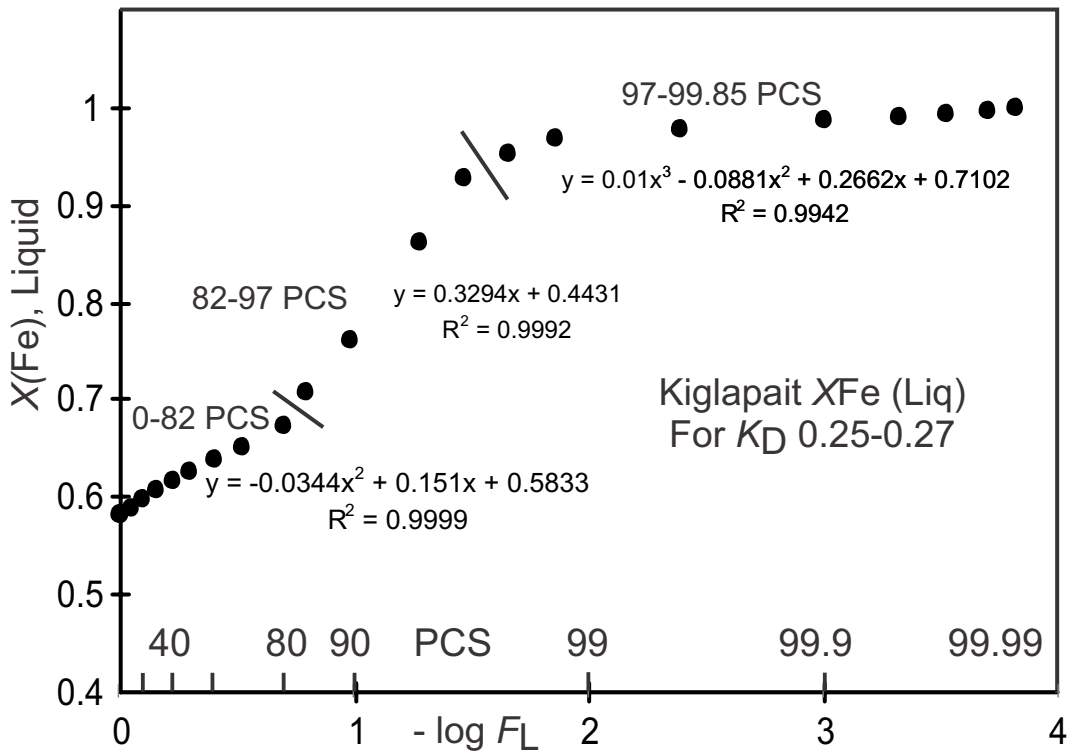

Morse Fig. 12

Always consult and cite the final, published document. See http://www.minsocam.org or GeoscienceWorld

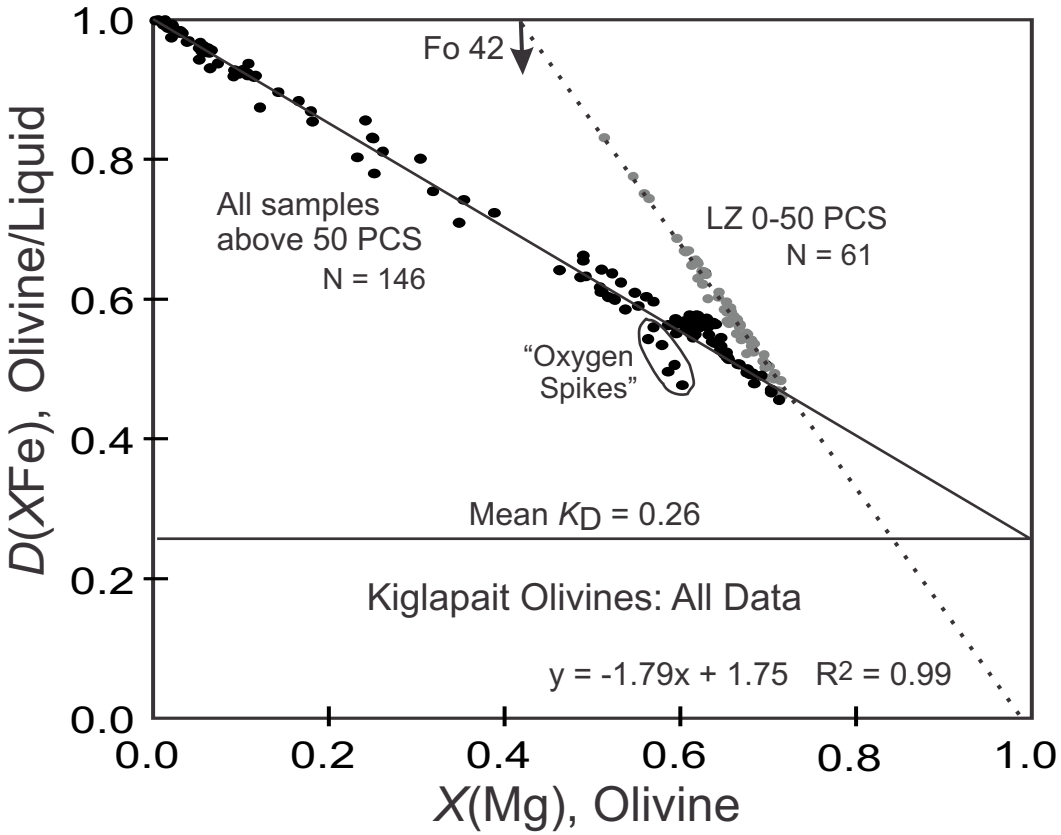
1.0
0.8
0.6
0.4
0.2
0.0
0.0
0.2
0.4
0.6
0.8
1.0
D(XFe), Olivine/Liquid
X(Mg), Olivine
Fo 42
All samples
above 50 PCS
N = 146
LZ 0-50 PCS
N = 61
"Oxygen
Spikes"
Mean KD = 0.26
Kiglapait Olivines: All Data
y = -1.79x + 1.75 R2 = 0.99

Morse Fig. 13

Table 1. Abbreviations used in the text

Ab	Albite
An	Anorthite
Aug	Augite
AUG	Oxygen-normative augite*
ΔH_f	Latent heat (enthalpy) of fusion
D	Partition coefficient
Di	Diopside
Fa	Fayalite
F_L	Volume fraction of system present as liquid
Fo	Forsterite
FSP	Oxygen-normative feldspar*
J	Joule
k	kilo-
K_D	Exchange coefficient
L	Liquid
LZ	Lower Zone
OL	Oxygen-normative olivine*
Opx	Orthopyroxene
Or	Orthoclase
P	Pressure
PCS	(volume) percent solidified in the Kiglapait intrusion
QUILF	Quartz-Ulvöspinel-Ilmenite-Fayalite equilibria (Andersen *et al.* 1993)
S	Solid
T	Temperature
UBZ	Upper Border Zone
UZ	Upper Zone
V	Vapor
X	Mole fraction

Note: *normative phases normalized to total AUG + FSP + OL

TABLE 2. LIST OF LINEAR PARTITIONING RESULTS May 14, 2014

A. Binary Solutions

Single Loop: Liquidus & Solidus

SYSTEM	K_D	P	SOURCE	COMMENTS
Fo-Fa Olivine	0.227	1-atm	Morse 1997 (Bowen & Schairer)	Small curve
An-Ab Plagioclase	0.282	1-atm	Morse 1997 (Bowen)	NOT linear
-do-	0.285	1-atm	Morse 2000 (Bowen)	Two segments
-do-	0.22	5 kb	Morse 2000 (Nekvasil)	Barely 2 segments
-do-	0.252	10 kb	Morse 1997 (Lindsley)	Two segments
-do-	0.276	1-atm	This study	Single curve
An-Ab-H_2O	0.05	5 kb	Morse 2000 (Nekvasil)	R^2 0.9997
Di-An-Ab	0.26	1-atm	Morse 1997 (Bowen, Kushiro)	Intercept 0.975
Basaltic Olivine	0.33	1-atm	Morse 1997 (Hoover-Irvine)	Variable K_D*
Augite - Olivine	0.32	1-atm	Morse 2001 (Selected range)	R^2 0.995

B. Three-Phase Systems

(1) Two crystal species plus liquid (Two binary S - L solutions and one S-S(L) where () signifies the saturating phase).

Augite - Olivine - Liquid			Based on Morse (1996; 2001)		
Augite - Liquid (Ol)	0.19	1-atm	This study		R^2 0.9995
Olivine - Liquid (Aug)	0.335	1-atm	This study	Variable K_D*	R^2 0.996
Augite - Olivine (L)	0.361	1-atm	This study		R^2 0.9972

(2) Two crystal species plus a third saturating phase: The pyroxene solvus (Lindsley, 1983).

Augite - Pigeonite	0.74	1-atm	This study	R^2 0.990
Augite - Opx	–NA--	1-atm	This study	R^2 0.01

C. Azeotropes in solid-liquid systems

(Binary solutions with a common invariant point between phases)

NaCl-KCl	0.215, 0.395	1-atm	Morse 1997 (Waldbaum) Classic precision
Ab-Or wt %	0.325, 0.417	1-atm	Morse 1997 (Waldbaum & Thompson) ditto
Ab-Or mol %	0.320, 0.417	1-atm	This study (Waldbaum & Thompson) ditto
Ab-Or-H_2O	0.04, 0.12	5 kb	Morse 2000 (Morse 1970)

D. Two solid phases

Magnesiowüstite - spinel	0.205	16-22 GPa, 1600 C	Morse 2000 (Matsuzaka)	
Chlorite - Garnet	0.162	Chlorite zone	Morse 2001 (Spear)	
Biotite - Garnet	0.25	Sillimanite zone	Morse 2001 (Kretz)	R^2 = 0.995
Synthetic van Laar loops	0.121-0.0077		Morse 2001 (Kretz)	R^2 ~ 1
Augite - Olivine as above				

E. Boiling Mixtures

1. Simple liquid-vapor systems. All data from Weishaupt (1975).

Methylcyclohexane -CCl4	0.514	1-atm	Morse 2000	R^2 0.9996
CCL4 - Acetone	Var.	0.600 bar	Morse 2000	NOT LINEAR

Many others not linear, listed in Table 1 of Morse (2000).

2. Azeotropes

Methanol-Chloroform	0.336, 0.182	1-atm	Morse 2000	R^2 >0.996
Toluol - Isobutanol	0.352, 0.306	1-atm	Morse 2000	>=0.9996

Many others linear listed in Table 1 of Morse (2000)

**D* flattens out at low Mg- high Fa: See also this study

Table 3. Liquid compositions for Kiglapait olivines

1996 Data PCS	-lgF(L)	X2S MAX XMg(OL)	X1S	NBO/T	KD	X1L XFe (Liq)
0	0	0.740	0.260	0.645	0.251	0.584
10	0.0458	0.734	0.266	0.658	0.252	0.590
20	0.0969	0.727	0.273	0.672	0.253	0.598
30	0.1549	0.719	0.281	0.687	0.254	0.606
40	0.2218	0.710	0.290	0.705	0.255	0.615
50	0.3010	0.700	0.300	0.724	0.257	0.625
60	0.3979	0.687	0.313	0.747	0.259	0.638
70	0.5229	0.672	0.328	0.775	0.261	0.652
80	0.6990	0.650	0.350	0.812	0.263	0.672
84	0.7959	0.610	0.390	0.830	0.264	0.708
89.5	0.9788	0.540	0.460	0.862	0.266	0.762
94.7	1.2757	0.374	0.626	0.904	0.268	0.862
96.6	1.4685	0.222	0.778	0.926	0.269	0.929
97.8	1.6576	0.153	0.847	0.942	0.269	0.954
98.6	1.8539	0.112	0.888	0.955	0.270	0.967
99.59	2.3872	0.075	0.925	0.966	0.270	0.979
99.9	3.0000	0.050	0.950	0.936	0.269	0.986
99.953	3.3279	0.036	0.964	0.901	0.268	0.990
99.98	3.6999	0.015	0.985	0.845	0.265	0.996
99.985	3.8239	0	1	0.822	0.264	1.000
99.99	4	0	1	0.787	0.261	1.000